ACS Catalysis

pubs.acs.org/acscatalysis Research Article

Mediating the Competitive Adsorption of Propane and Oxygen via Pt-Sulfate Synergy for Enhanced Propane Combustion

Han Zhao,[#] Lu Liu,[#] Yao-Dong Hao, Xiao-Yang Zhu, Qian Zhou, Yi-Wei Xian, Wen-Zhi Jia,* Lin Dong, Meng-Fei Luo, Wei Tan,* and Jian Chen*

Cite This: *ACS Catal.* 2025, 15, 21054−21065 Read Online

ACCESS | Metrics & More | Article Recommendations | Supporting Information

ABSTRACT: Developing efficient catalysts for the low-temperature combustion of short-chain alkane VOCs remains challenging. One of the primary obstacles to further enhancing catalytic combustion performance is believed to be the inherently weak adsorption of alkanes, which leads to their loss in competitive adsorption against O_2 on reactive sites. Although sulfate-modified Pt catalysts have demonstrated potential for short-chain alkane combustion, the reaction mechanism on those catalysts, particularly concerning the adsorption behaviors of the reactants, remains unclear. Herein, starting from the preparation of sulfated ZrO_2 through an eco-friendly simultaneous pyrolysis strategy, an efficient supported Pt catalyst (Pt/ZrO_2-5S) for propane combustion was prepared. Compared to Pt supported on bare ZrO_2 (Pt/ZrO_2), Pt/ZrO_2-5S displayed significantly promoted activity for propane combustion, achieving a T_{90} of 200 °C, which was 120 °C lower than that of Pt/ZrO_2 (320 °C). This dramatic improvement implied the critical role of Pt-sulfate synergy in altering propane adsorption/dissociation and oxygen adsorption. Further systematic characterizations, kinetic studies, and theoretical calculations disclosed that the sulfate species could efficiently facilitate the activation/cleavage of the C−H bond of propane and the adsorption of the resulting intermediate (e.g., C_3H_7*), while simultaneously weakening oxygen adsorption. The synergistic regulation of C_3H_8 and O_2 adsorption for alleviating competitive adsorption provides a clear explanation for the superior activity on sulfate-modified Pt catalysts in propane combustion. This work offers fundamental insights into the design of efficient catalysts for alkane combustion through tailoring adsorption behavior.

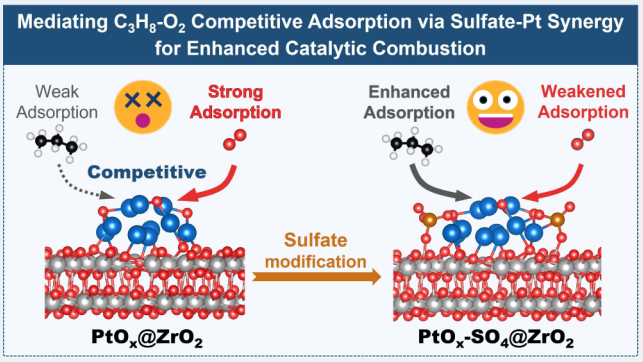

KEYWORDS: *propane combustion, Pt-based catalyst, acid modification, competitive adsorption, reaction mechanism*

1. INTRODUCTION

Catalytic combustion is generally accepted as one of the most effective technologies for VOCs elimination.[1−6] Among various VOCs with distinct molecular structures, short-chain alkanes, emitted by the petrochemical industry and vehicles, pose particular challenges for catalytic combustion elimination due to the stable C−C and C−H bonds.[7−16] In recent decades, propane has been intensively adopted as a model short-chain alkane for catalyst performance evaluation, owing to its role as a primary component of liquefied petroleum gas (LPG) and a significant hydrocarbon pollutant in exhaust gas.[17−21] Despite considerable progress in catalyst development, achieving complete propane combustion at low temperatures (<200 °C) continues to be a major hurdle.[22,23]

To date, the reported works to construct robust catalysts for propane combustion have mainly focused on altering the structure and chemical states of active sites, engineering the support, and selecting appropriate promoters.[17,24−29] For instance, Ge et al. found that the catalytic performance of Pt catalysts supported on CeO_2 (100) facet for propane oxidation was primarily governed by the electronic state of the Pt species when Pt particle size was below 4 nm. In contrast, the geometric structure of Pt particles became the determining factor as the particle size exceeded 4 nm, since metallic Pt species particles became predominant on larger Pt particles.[26] Xia et al. proposed a feasible strategy to adjust the metal bond lengths within Pd clusters through substituting partial Pd with smaller transition metals, which significantly promoted the activation of low-energy C−C bonds within propane.[30] Yang et al. claimed that Brønsted acid sites of the support help reduce water coverage on the Pt surface through a spillover-like mechanism, enabling more available sites for propane adsorption and activation.[31] It was also reported that acid

Received: September 8, 2025
Revised: December 1, 2025
Accepted: December 2, 2025

https://doi.org/10.1021/acscatal.5c06403
ACS Catal. 2025, 15, 21054−21065

sites could stabilize the metallic Pt species, which served as efficient reactive sites for C−H activation.[3,32−34] Yet, it should be noticed that metallic Pt species show a higher affinity for O_2 compared to propane, which possibly results in the severe competitive adsorption between propane and oxygen, thus suppressing the kinetics of the combustion reaction.[35−37] Therefore, enhancing the adsorption of propane on active sites should be critical to increase the catalytic activity. Yu et al. constructed the electron-enriched $Pt^{\delta+}$ species to facilitate the propane adsorption and methyl C−H cleavage, which boosted propane oxidation.[22] Dong et al. also found that the electron-deficient Pt sites are decisive to propane adsorption/activation.[9,38] Chen et al. proposed that sulfate incorporation into Pt/TiO_2 catalyst generates a (Pt−S−O)-Ti active structure, which serves as the primary active sites for propane combustion, and the active oxygen atoms in this structure play a critical role in propane adsorption and activation.[39] However, to the best of our knowledge, few studies have discussed the impact of competitive adsorption between propane and adsorption with O_2 on the catalytic combustion activity in detail. Gaining deeper insight into the critical role of reactant adsorption behavior would benefit the design of efficient catalysts for propane combustion.

In this work, building upon previous advances in constructing robust Pt catalysts for the catalytic combustion of short-chain alkane combustion by sulfate modification strategy,[40−50] we further developed sulfate-modified Pt catalyst supported on ZrO_2. The sulfate species were introduced through an environmentally friendly simultaneous pyrolysis of $(NH_4)_2SO_4$ during the preparation of the ZrO_2 support, offering a facile and cost-effective acid modification strategy for Pt catalysts compared to the application of transition metal oxides (e.g., MoO_3, WO_3, and Nb_2O_5). The sulfate-modified Pt/ZrO_2 catalyst was found to exhibit superior low-temperature propane oxidation activity, with a T_{90} as low as 200 °C. In addition, using the sulfate-modified Pt/ZrO_2 catalyst and its unmodified Pt/ZrO_2 counterpart as model catalysts, the impact of adsorption behaviors of propane and oxygen on catalytic combustion performance was further investigated by the combination of characterizations, kinetic studies, and theoretical calculations. It was found that the weak adsorption of propane and its inferior competitive adsorption against O_2 on Pt accounted for the relatively low propane combustion activity over Pt/ZrO_2. In contrast, sulfate modification significantly promoted propane activation and enhanced its adsorption while simultaneously weakening oxygen adsorption. This effectively mediated the competitive adsorption between propane and O_2, thereby enabling highly efficient propane combustion over sulfate-modified Pt/ZrO_2.

2. EXPERIMENTAL SECTION

2.1. Chemicals and Reagents. $Zr(CO_3)_2$ was purchased from Shanghai Diyang Chemical Co., Ltd. $(NH_4)_2SO_4$ was obtained from Sinopharm Chemical Reagent Co., Ltd. $Pt(NO_3)_2$ solution was brought from Sino Chemical Reagent Co., Ltd. Other reagents are of analytical grade and used without further purification.

2.2. Preparation of ZrO_2- and Sulfate-Modified ZrO_2 Supports. ZrO_2 support was prepared by calcining zirconium carbonate ($Zr(CO_3)_2$) in a muffle furnace at 550 °C for 3 h with a heating rate of 10 °C min^{-1}. The resulting powder, consisting of a mixture of tetragonal ZrO_2 and monoclinic ZrO_2, was designated as ZrO_2.

The sulfated ZrO_2 was prepared by an eco-friendly and facile simultaneous pyrolysis method from $(NH_4)_2SO_4$ with $Zr(CO_3)_2$, without the generation of any liquid waste. Specifically, 4 g of $Zr(CO_3)_2$ was mixed with predetermined quantities of $(NH_4)_2SO_4$ (0.10, 0.20, 0.28, 0.80 g) and then ground for 45 min. Subsequently, the resultant mixture was calcined under conditions identical with those used for the preparation of ZrO_2. The obtained sulfated ZrO_2 was denoted as ZrO_2-xS (x = 2.5, 5, 7, and 20, x% represents the mass ratio of $(NH_4)_2SO_4$ to $Zr(CO_3)_2$). Pt species were loaded on the ZrO_2 and ZrO_2-xS supports by using the wetness impregnation method. Typically, 1 g of support was immersed in $Pt(NO_3)_2$ solution (5 mL, 0.002 g_{Pt}·mL^{-1}) and kept for 3 h at room temperature. Afterward, the solvent was evaporated at 90 °C, and the resulting powder was further dried in an oven at 100 °C for 1 h, followed by calcination at 500 °C for 4 h with a ramping rate of 10 °C·min^{-1}. The prepared Pt catalysts supported on ZrO_2 and ZrO_2-xS were named Pt/ZrO_2 and Pt/ZrO_2-xS, respectively. For better understanding, the synthesis flowchart of Pt/ZrO_2-xS can be found in Figure S1. In addition, for comparison, the Pt-$5SO_4^{2-}/ZrO_2$ catalyst was prepared by a traditional method, involving impregnating ZrO_2 with sulfuric acid, followed by calcination and subsequent loading of 1 wt% Pt.

In order to investigate the influence of the phase structure of the ZrO_2 support on the catalytic performance of Pt catalysts, Pt catalysts supported on tetragonal ZrO_2 (t-ZrO_2) and monoclinic ZrO_2 (m-ZrO_2) without sulfate modification were also prepared as references, which were denoted as Pt/t-ZrO_2 and Pt/m-ZrO_2, respectively. Detailed information on preparing Pt/t-ZrO_2 and Pt/m-ZrO_2 was provided in Supporting Information (Text S1).

2.3. Characterization. The Brunauer-Emmet-Teller (BET) specific surface area of the catalysts was determined by N_2 physisorption at 77 K by using a JW-BK 200 C apparatus. Prior to the measurement, the catalyst was degassed at 120 °C for 4 h to remove adsorbed water and impurities. The specific surface area was determined from 10 data points in the relative pressure (P/P_0) range 0.03−0.35 on the adsorption isotherm. X-ray fluorescence (XRF) analysis was conducted to determine the actual contents of Pt and S elements, using a Shimadzu XRF-1800 spectrometer. Thermogravimetry (TG) analysis was performed on a NETZSCH STA 449F3 instrument with a temperature range of 30 to 800 °C (10 °C·min^{-1}) in an air flow (20 mL·min^{-1}). The powder X-ray diffraction (XRD) patterns of the catalysts were recorded using a Bruker D8 diffractometer with Cu Kα radiation (operating at 40 kV and 40 mA), with a scanning rate of 12°·min^{-1} over a 2θ range of 10−90°. Raman spectroscopy spectra were collected on a Renishaw in Via Reflex confocal microprobe Raman system (excitation wavelength: 325 nm, laser power: 10 mW, acquisition time: 30 s, number of scans: 100, resolution: 1 cm^{-1}). The NH_3-temperature-programmed desorption (NH_3-TPD) test was carried out in a tubular quartz reactor. Prior to the test, the catalyst (50 mg, 60−80 mesh) was put into the reactor and then pretreated by a N_2 flow (20 mL·min^{-1}) at 300 °C for 30 min to remove adsorbed water and impurities, followed by cooling to 50 °C. Subsequently, high-purity NH_3 gas (30 mL·min^{-1}) was introduced into the reactor for 5 min, and then the system was purged with a N_2 flow (20 mL·min^{-1}) for 30 min to remove gaseous NH_3 or physically adsorbed NH_3. Afterward, the reactor was heated from 40 to 700 °C at a heating rate of 10 °C·min^{-1} under a

https://doi.org/10.1021/acscatal.5c06403
ACS Catal. 2025, 15, 21054−21065

high-purity N_2 flow (20 mL·min^{-1}) to desorb chemically adsorbed NH_3. The desorbed NH_3 in the outlet gas was detected by a thermal conductivity detector (TCD). The total number of surface acid sites of the catalyst was quantified by calibrating the TCD response with known NH_3 quantities, where the integrated peak area of the desorption profile was linearly correlated with the amount of chemisorbed NH_3. Pyridine adsorption Fourier-transform infrared (pyridine-IR) spectra were recorded on SHIMADZU ITRracer-100 spectrometer to study the type of acid sites in catalysts. Prior to the test, the wafer of catalyst was pretreated at 300 °C under vacuum condition for 0.5 h. Afterward, the wafer was cooled to 50 °C and saturated adsorbed by pyridine for 15 min. The pyridine-IR spectra of the wafers were collected in the spectral range 2000−1200 cm^{-1} with 64 scans after desorption of pyridine at 100 °C for 1 h under a dynamic vacuum (10−2 bar). Electron paramagnetic resonance (EPR) test was conducted on Bruker EPR EMXplus under 9.8 GHZ. X-ray photoelectron spectra (XPS) were recorded using an ESCALAB 250Xi instrument with a monochromatic Al anode Kα radiation (hυ = 1486.6 eV) as the excitation light source, using a spot size of 500 mm. The narrow scan spectra were collected using a pass energy of 30 eV with a step size of 0.1 eV, and the binding energy was calibrated by C 1*s* XPS centered at 284.8 eV. XPS fitting was performed using CasaXPS Version 2.3.24 software, and the Shirley background was applied for spectra analysis. High-resolution transmission electron microscopy (HRTEM) and scanning transmission electron microscopy (STEM) images of the catalyst were obtained by a JEOL JEM-2100 F Field-Emission Transmission Electron Microscope operating at 200 kV, and elemental mapping was analyzed by EDAX Energy Dispersive Spectrometer (EDS). *In situ* diffuse reflectance infrared spectroscopy (DRIFTS) of propane combustion/adsorption experiments were carried out on a Thermal-Fischer Nicolet iS50 FTIR spectrometer equipped with an MCT detector. In a typical process, 20 mg catalyst was loaded into a PIKE DRIFT accessory and pretreated in a flow of 2 vol% O_2/N_2 balanced at 380 °C for 30 min, then background spectra were recorded at the desired temperatures in an N_2 flow. Afterward, a mixed flow of 0.2 vol% C_3H_8 + 2 vol% O_2 (when used) + N_2 was introduced, and the spectra were recorded. Propane dehydrogenation performance was evaluated using temperature-programmed reactions in a C_3H_8 flow (2000 ppm) from room temperature to 400 °C (2 °C·min^{-1}). The composition of the outlet gas was continuously analyzed using an online flue gas analyzer equipped with an infrared sensor (measurement range = 0−4000 ppm, resolution = 1 ppm). C_3H_8-temperature-programmed desorption (C_3H_8-TPD) test was carried out in a tubular quartz reactor. The pretreatment on the catalyst (50 mg, 60−80 mesh) was the same as that for NH_3-TPD. After the pretreatment, 5% C_3H_8/Ar flow (30 mL·min^{-1}) was introduced into the reactor for 20 min at 40 °C, and then the system was purged with an N_2 flow (20 mL·min^{-1}) for 30 min to remove gaseous C_3H_8 or physically adsorbed C_3H_8. Afterward, the reactor was heated from 40 to 500 °C (10 °C·min^{-1}) under a high-purity He flow (30 mL·min^{-1}) to desorb chemically adsorbed C_3H_8, which was detected by a TCD.

2.4. Catalytic Activity Evaluation. The catalytic performance was evaluated in a homemade quartz tube reactor (*i.d.* = 6 mm). Typically, 50 mg of catalyst was loaded and subjected to a reactant gas mixture (0.2 vol% C_3H_8 + 2 vol% O_2 balanced with N_2) at a total flow rate of 66.66 mL·min^{-1}, corresponding to a weight hourly space velocity (WHSV) of 80,000 mL·g^{-1}·h^{-1}. Propane concentrations in the inlet ($[C_3H_8]_{in}$) and outlet ($[C_3H_8]_{out}$) gases were analyzed by using a Shimadzu GC-2014 gas chromatograph equipped with an HP-GS-GASPRO capillary column (30 m × 0.25 mm × 0.25 μm) and FID detector. Propane conversion at the desired temperature was calculated using the following formula:

$$C_3H_8 \text{ conversion} = ([C_3H_8]_{in}\text{-}[C_3H_8]_{out})/[C_3H_8]_{in} \times 100\% \quad (1)$$

The concentrations of CO_2 ($[CO_2]_{out}$) and CO ($[CO]_{out}$) in the outlet gas were also analyzed during the activity test. It was found that no CO was detected in the outlet gas, and the CO_2 selectivity calculated based on the concentration of CO_2 in the outlet gas was 100%.

$$CO_2 \text{ selectivity} = 3^*[CO_2]_{out}/([C_3H_8]_{in} - [C_3H_8]_{out}) \times 100\% \quad (2)$$

In kinetic tests, propane conversion was controlled below 15% in order to eliminate mass and heat transfer limitations. The apparent activation energy (E_a) was obtained by determining the catalyst activity at different temperatures, and the number of corresponding reaction stages was determined in the partial pressure ranges of oxygen (1.515−9.09 kPa) and propane (0.202−0.808 kPa). Specific experimental data are given in the Supporting Information.

2.5. Computational Method. Vienna Ab Initio Simulation Package (VASP)[51,52] was employed to perform all the density functional theory (DFT) calculations within the generalized gradient approximation (GGA) using the PBE formulation.[53] The projected augmented wave (PAW) potentials[54,55] were chosen to describe the ionic cores and take valence electrons into account using a plane wave basis set with a kinetic energy cutoff of 400 eV. Partial occupancies of the Kohn−Sham orbitals were allowed using the Gaussian smearing method and a width of 0.05 eV. The electronic energy was considered self-consistent when the energy change was smaller than 10^{-5} eV. A geometry optimization was considered convergent when the force change was smaller than 0.02 eV/Å. Grimme's DFT-D3 methodology was used to describe the dispersion interactions.[56]

The equilibrium lattice constants of the tetragonal ZrO_2 unit cell were optimized to be a = 3.610 Å and c = 5.230 Å. We then used it to construct a ZrO_2 (011) surface model with $p(3 \times 2)$ periodicity in the X and Y directions and 2 stoichiometric layers in the Z direction, separated by a vacuum layer in the depth of 15 Å in order to separate the surface slab from its periodic duplicates. This model comprises 24 Zr and 48 O atoms. Model 1 was built by adding one $Pt_{10}O_3$ cluster onto it. Model 2 was built by adsorbing one SO_4 radical onto Model 1. During structural optimizations, a 2 × 2 × 1 k-point grid in the Brillouin zone was used for k-point sampling, and the bottom stoichiometric layer was fixed while the top one was allowed to relax.

The adsorption energy (E_{ads}) of adsorbate A was defined as $E_{ads} = E_{A/surf} - E_{surf} - E_{A(g)}$ (3). $E_{A/surf}$, E_{surf} and $E_{A(g)}$ are the energy of adsorbate A adsorbed on the surface, the energy of the clean surface, and the energy of the isolated A molecule in a cubic periodic box with a side length of 20 Å, respectively.

https://doi.org/10.1021/acscatal.5c06403
ACS Catal. 2025, 15, 21054−21065

3. RESULTS AND DISCUSSION

3.1. Construction of Pt/ZrO_2- and Sulfate-Modified Pt/ZrO_2Catalysts. The structures of ZrO_2 and ZrO_2-xS supports, as well as the supported Pt catalysts, were first investigated. As listed in Table 1, the specific surface area of Pt/ZrO_2-xS catalysts increased first and then decreased with the increase in sulfate content. Pt/ZrO_2-5S showed the highest surface area of 26 $m^2 \cdot g^{-1}$, whereas Pt/ZrO_2-20S exhibited the lowest surface area of 3 $m^2 \cdot g^{-1}$. Moreover, the content of sulfur in Pt/ZrO_2-xS increased as expected with the addition of more $(NH_4)_2SO_4$ when preparing a sulfated ZrO_2 support, and the actual Pt loading is close to the theoretical value, as indicated by the results of XRF. Moreover, the sulfate loss for Pt/ZrO_2-xS catalysts (ca. 50%) during the preparation was much less than that for Pt-5SO_4^{2-}/ZrO_2 catalyst (93.3%) prepared by depositing Pt onto sulfuric acid-impregnated ZrO_2 (Table S1), further underscoring the advantage of the one-step preparation method in terms of environmental friendliness. In addition, the thermogravimetric (TG) experiment revealed that the sulfate species in Pt/ZrO_2-5S remained stable up to *ca.* 600 °C (Figure S2).

Table 1. Physicochemical Properties of Pt/ZrO_2 and Pt/ZrO_2-xS Catalysts

		Element content[b]					
		Pt		S			
Catalysts	SSA ($m^2 \cdot g^{-1}$)[a]	(wt %)	(mmol·g^{-1})	(wt %)	(mmol·g^{-1})	Total amount of surface acid sites (μmol·g^{-1})[c]	TOF_{Pt} ($10^{-2} \cdot s^{-1}$)[d]
$PtZrO_2$	21	1.00	0.050	0	0	13.9	0.24
Pt/ZrO_2-2.5S	23	1.01	0.052	0.55	0.17	36.5	3.5
Pt/ZrO_2-5S	26	0.99	0.051	1.00	0.31	202	17.7
Pt/ZrO_2-7S	13	0.96	0.049	1.50	0.47	56.5	5.8
Pt/ZrO_2-20S	3	0.99	0.051	4.43	1.38	28.1	2.4

[a]Specific surface area (SSA) was measured by N_2 adsorption−desorption analysis at 77 K. [b]Actual Pt and S contents were determined by XRF. [c]The total acid site amount was calculated from NH_3-TPD profiles. [d]The TOF_{Pt} was calculated using the formula of $TOF_{Pt} = r \times M_{Pt}/D$, where r is the specific mass reaction rate at 200 °C, M_{Pt} is the molar mass of Pt (195 $g_{Pt} \cdot mol^{-1}$), and D is the dispersion of Pt ($D = 1.12/d$, d (nm) is the average size of Pt particles obtained from HRTEM images).

Figure 1a illustrated the XRD patterns of supported Pt catalysts, which are consistent with the XRD patterns of the corresponding supports (Figure S3), suggesting that the loaded Pt hardly altered the crystal structure of the ZrO_2 support. ZrO_2 and Pt/ZrO_2 were found to consist of both tetragonal ZrO_2 (PDF# 50−1089) and monoclinic ZrO_2 (PDF# 37−1484).[25,57] Notably, the characteristic diffraction peaks assigned to monoclinic ZrO_2 gradually diminished with the addition of more sulfate species, and the XRD peaks for Pt/ZrO_2-5S and Pt/ZrO_2-7S were all attributed to tetragonal ZrO_2. However, ZrO_2-20S and Pt/ZrO_2-20S showed an amorphous structure. NH_3-TPD experiments were conducted to evaluate the surface acidity of the prepared Pt catalysts (Figure 1b), and the total amount of surface acid sites was calculated (Table 1). All Pt/ZrO_2-xS catalysts possessed more surface acid sites than Pt/ZrO_2 due to the presence of sulfate species. Pt/ZrO_2-5S possessed the most acid sites of 202 μmol·g^{-1}, which was almost 15 times that of Pt/ZrO_2 (13.9 μmol·g^{-1}). The lower specific surface area of Pt/ZrO_2-7S and Pt/ZrO_2-20S likely explained their reduced number of surface acid

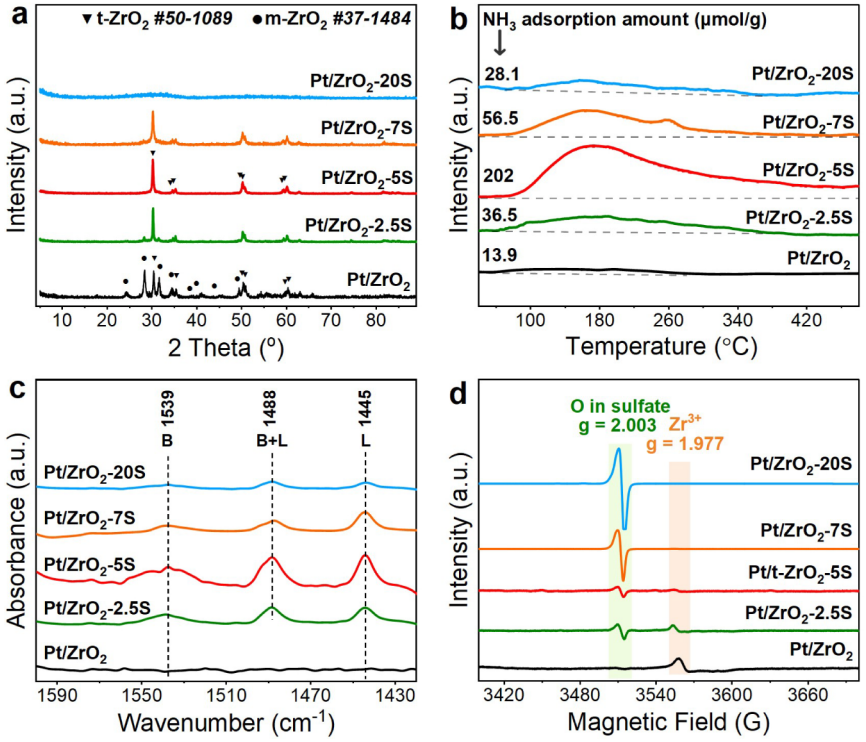

Figure 1. a) XRD patterns, b) NH_3-TPD profiles, c) Py-IR spectra, and d) EPR spectra for Pt catalysts.

https://doi.org/10.1021/acscatal.5c06403
ACS Catal. 2025, 15, 21054−21065

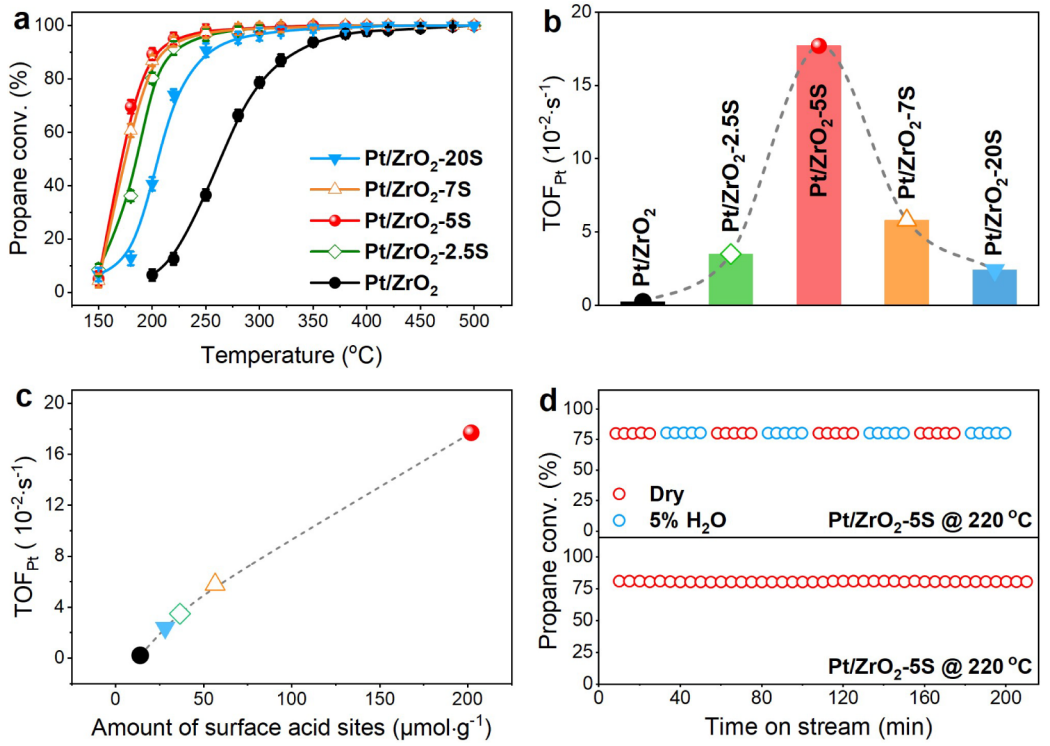

Figure 2. a) Light off curves and b) TOF_{Pt} of Pt catalysts in the propane combustion reaction. c) Relationship between TOF_{Pt} and the amount of surface acid sites. d) Stability evaluation on Pt/ZrO_2-5S.

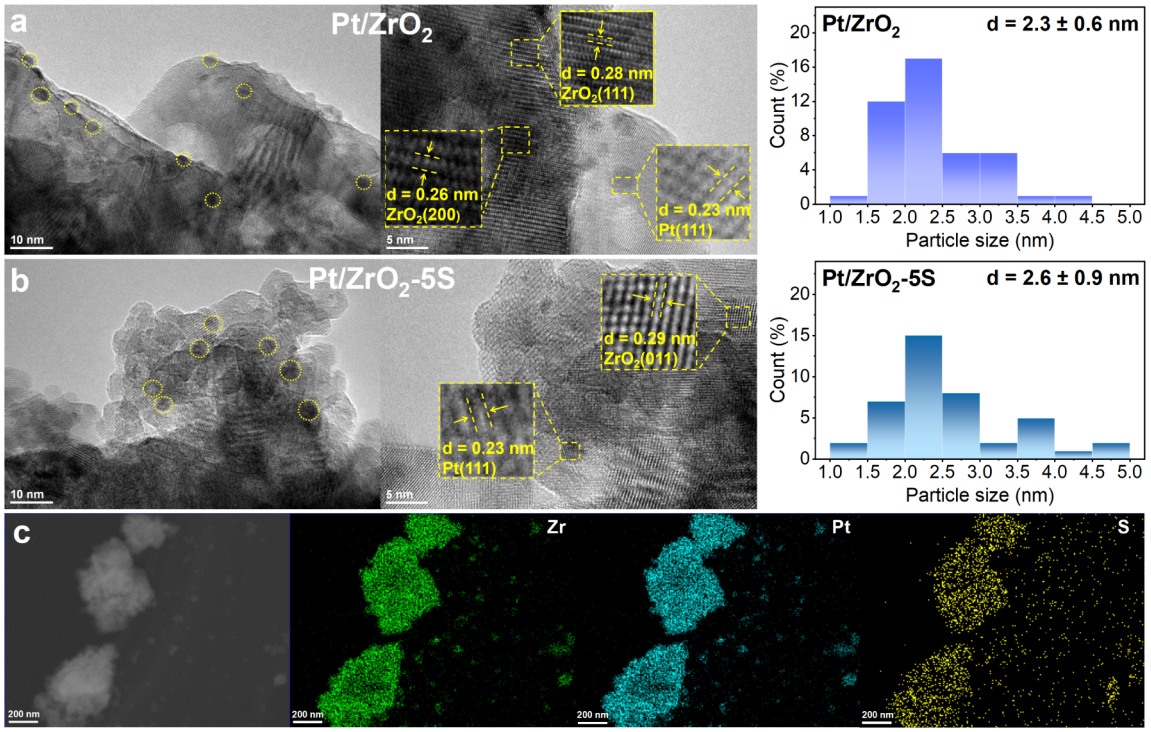

Figure 3. HRTEM images of a) Pt/ZrO_2 and b) Pt/ZrO_2-5S, and the size distribution of Pt nanoparticles, and c) STEM image and corresponding elemental EDS mapping images of Pt/ZrO_2-5S.

sites compared to Pt/ZrO_2-5S. Py-IR spectra revealed that both Lewis acid and Brønsted acid sites coexisted on Pt/ZrO_2 and Pt/ZrO_2-*x*S, with Lewis acid sites being dominant (Figure 1c). Electron paramagnetic resonance (EPR) spectra were also recorded to gain more structural information (Figure 1d). In addition to the signal ascribed to the Zr^{3+} species (g = 1.977), a signal at g = 2.003 corresponding to oxygen species in sulfate also appeared on Pt supported on sulfated ZrO_2.[58] The monotonic increase in the intensity of the signal at g = 2.003 for Pt/ZrO_2-*x*S with increasing $(NH_4)_2SO_4$ addition during

https://doi.org/10.1021/acscatal.5c06403
ACS Catal. 2025, 15, 21054−21065

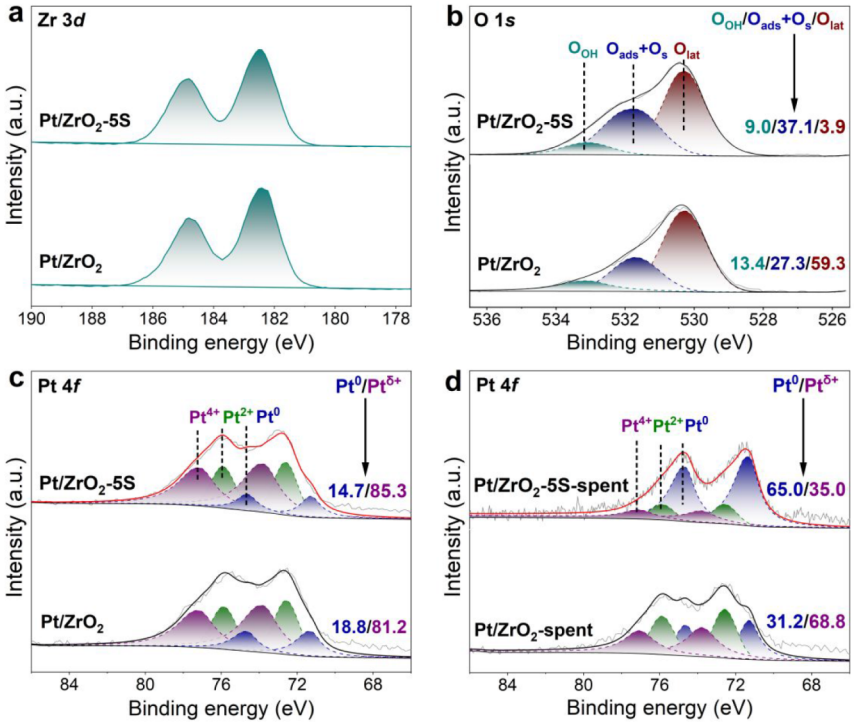

Figure 4. a) Zr 3*d* and b) O 1*s* XPS of Pt/ZrO_2 and Pt/ZrO_2-5S, Pt 4*f* XPS of c) fresh and d) spent Pt/ZrO_2 and Pt/ZrO_2-5S.

preparation correlated well with the XRF data (Table 1). Moreover, the attenuated EPR signal at g = 1.977 on Pt/ZrO_2-*x*S indicated a reduction in Zr^{3+} concentration, resulting from the electron-withdrawing inductive effect of sulfate groups.

3.2. Catalytic Performance in Propane Combustion Reaction. Figure 2 showed the results of catalytic performance evaluation of Pt catalysts in the propane combustion reaction. Notably, the addition of sulfate species to Pt/ZrO_2 catalysts significantly promoted propane combustion activity, as shown in the light-off curves (Figure 2a). Specifically, with the increase in S content, propane combustion activity on Pt catalysts first rose and then decreased with the increasing amount of sulfate species. Pt/ZrO_2-5S performed the best among the serial sulfate-modified Pt/ZrO_2 catalysts, achieving a T_{90} (the temperature at which propane conversion reached 90%) as low as 200 °C, which was 120 °C lower than that of Pt/ZrO_2 (320 °C). Additionally, the turnover frequency of Pt sites (TOF_{Pt}) on Pt/ZrO_2 and Pt/ZrO_2-*x*S was calculated to evaluate the intrinsic activity of Pt active sites (Table 1 and Figure 2b). The TOF_{Pt} of the series Pt catalysts followed an order of Pt/ZrO_2-5S > Pt/ZrO_2-7S > Pt/ZrO_2-2.5S > Pt/ZrO_2-20S > Pt/ZrO_2. Since the introduction of sulfate species to Pt/ZrO_2 significantly enhanced its surface acidity, the relationship between TOF_{Pt} and the surface acid site amount was explored. As shown in Figure 2c, TOF_{Pt} exhibited a positive correlation with the amount of surface acid sites, suggesting the critical role of surface acid sites in enhancing the propane combustion activity on the Pt sites. Besides, the stability of Pt/ZrO_2-5S was studied under both dry and wet (5 vol% H_2O) conditions. The results demonstrated that water vapor hardly affected the catalytic performance of Pt/ZrO_2-5S in a long-term test, indicating its superior H_2O resistance and durability. Moreover, Pt/ZrO_2-5S also exhibited slightly higher propane oxidation activity than Pt-$5SO_4^{2-}/ZrO_2$ prepared by sequentially impregnating sulfuric acid and Pt onto ZrO_2, as shown in Figure S4.

As indicated by XRD (Figure S3) and Raman spectra (Figure S5), ZrO_2 in Pt/ZrO_2 was a mixture of tetragonal ZrO_2 and monoclinic ZrO_2, while ZrO_2 in Pt/ZrO_2-5S was in the tetragonal phase. To rule out the possibility that the superior propane combustion activity on Pt/ZrO_2-5S was more dependent on the crystal phase, Pt catalysts supported on pure tetragonal ZrO_2 (Pt/t-ZrO_2) and monoclinic ZrO_2 (Pt/m-ZrO_2) were prepared. It was found that Pt/t-ZrO_2 and Pt/m-ZrO_2 showed comparable propane combustion activity to Pt/ZrO_2 (Figure S6), confirming that the crystal phase of ZrO_2 was not the key factor in determining the catalytic performance of the Pt/ZrO_2 catalyst in this work.

3.3. Surface Structure and Chemical States. HRTEM images were collected to study the structure and morphology of Pt/ZrO_2 and Pt/ZrO_2-5S, as shown in Figure 3 and Figure S7. It was found that both Pt/ZrO_2 and Pt/ZrO_2-5S exhibited irregular morphologies, and Pt nanoparticles were clearly identified on the catalyst surface. Moreover, the measured lattice spacings of 0.28 and 0.26 nm on Pt/ZrO_2 were ascribed to the t-ZrO_2 (111) and m-ZrO_2 (200) facets, respectively, aligning well with the XRD analysis. For Pt/ZrO_2-5S, the measurement of lattice spacing (0.29 nm) indicated that the ZrO_2 support in Pt/ZrO_2 was in the t-ZrO_2 phase. The lattice space of 0.23 nm appearing in both Pt/ZrO_2 and Pt/ZrO_2-5S was related to the Pt (111) facet. According to the results of statistical analysis (Figure 3), the average Pt particle sizes for Pt/ZrO_2 and Pt/ZrO_2-5S were 2.3 and 2.6 nm, respectively. In addition, Pt/ZrO_2-20S with the most sulfate species, also exhibited a comparable Pt particle size of 2.7 nm (Figure S8). This result indicated that the sulfate content had a limited effect on the Pt dispersion. Besides, the elemental mapping images of Pt/ZrO_2-5S illustrated the uniform distribution of both Pt and S elements on the catalyst surface (Figure 3c).

https://doi.org/10.1021/acscatal.5c06403
ACS Catal. 2025, 15, 21054−21065

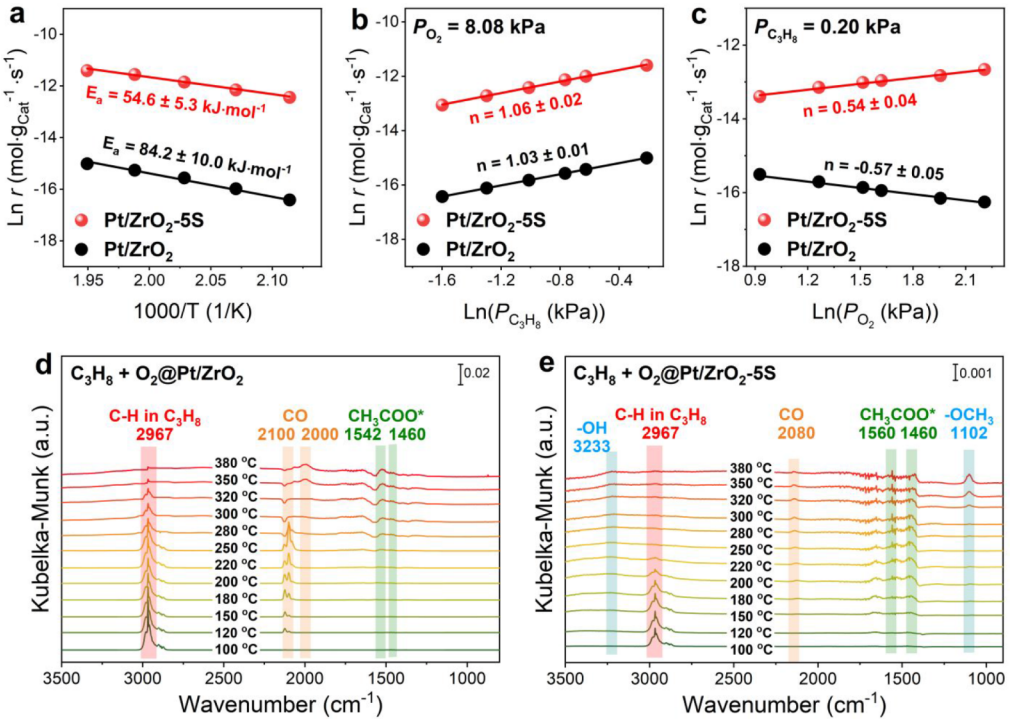

Figure 5. a) Arrhenius plots for Pt/ZrO_2 and Pt/ZrO_2-5S. Dependence of the reaction rate on the partial pressure of b) C_3H_8 and c) O_2 over Pt/ZrO_2 and Pt/ZrO_2-5S. *In situ* DRIFTS of propane combustion over d) Pt/ZrO_2, and e) Pt/ZrO_2-5S at different temperatures.

XPS spectra were recorded to study the chemical state of surface elements (Zr, O, S, and Pt). For Zr 3*d* XPS (Figure 4a and Figure S9), the components with binding energy at 182.5 and 184.9 eV are ascribed to Zr $3d_{5/2}$ and Zr $3d_{3/2}$, respectively.[59,60] This also implies that Zr species in the catalysts are mainly in the form of Zr^{4+}. Due to the high symmetry of Zr $3d_{5/2}$ and Zr $3d_{3/2}$ peaks, it was difficult to investigate the possible existence of Zr^{3+} based on XPS. Instead, here, EPR analysis was used to reveal the change of Zr^{3+} species content in Pt/ZrO_2-*x*S catalysts, as discussed in Figure 1d. The O 1*s* XPS of Pt/ZrO_2 demonstrated three distinct peaks with binding energies at 530.3, 531.7, and 533.1 eV (Figure 4b), corresponding to ZrO_2 lattice oxygen (Zr−O), adsorbed oxygen species (O_{ads}), and surface hydroxyl groups (O_{OH}), respectively.[61,62] The introduction of sulfate species significantly increased the intensity of the peak at 531.7 eV (Figure 4b and Figure S10), as the XPS peak of oxygen in sulfate species (O_S) exhibited a similar binding energy as that of O_{ads} species. S 2*p* XPS of sulfate-modified Pt catalysts showed two peaks at 168.9 and 170 eV (Figure S11), which were assigned to S $2p_{1/2}$ and S $2p_{3/2}$ states of S^{6+} species.[41]

Generally, the chemical states of Pt active sites are decisive to their catalytic performance in propane combustion reaction.[63] Therefore, Pt 4*f* XPS for fresh and spent Pt/ZrO_2 and Pt/ZrO_2-5S were recorded, as shown in Figure 4c and 4d. The components with binding energies of 71.3 and 74.7 eV corresponded to the Pt $4f_{7/2}$ and Pt $4f_{5/2}$ states of the Pt^0 species, respectively. The components with binding energies of 72.6 and 75.9 eV were ascribed to the Pt $4f_{7/2}$ and Pt $4f_{5/2}$ states of the Pt^{2+} species, respectively. The components with binding energies of 73.8 and 77.2 eV were related to the Pt $4f_{7/2}$ and Pt $4f_{5/2}$ states of Pt^{4+} species, respectively.[25,64] The results of Pt 4*f* spectra implied that Pt species existed in both oxidized ($Pt^{\delta+}$ = Pt^{2+} + Pt^{4+}) and metallic (Pt^0) forms in fresh and spent Pt/ZrO_2 and Pt/ZrO_2-5S, and metallic Pt species were not dominant for the fresh catalysts (18.8% and 14.7%). Notably, the proportion of metallic Pt species (Pt^0) on Pt/ZrO_2 and Pt/ZrO_2-5S increased after the catalytic performance evaluation, which should be due to the reduction of oxidized Pt species by reductive propane and its resulting intermediates.[18,25] Moreover, the increase in the Pt^0 proportion on Pt/ZrO_2-5S (from 14.7% to 65.0%) was more remarkable than that on Pt/ZrO_2 (from 18.8% to 31.2%), suggesting that the interaction between sulfate species and Pt could better induce the reduction of $Pt^{\delta+}$ during the propane oxidation reaction. Considering that metallic Pt active sites were known to be better for propane activation,[63,65] the generation of more Pt^0 sites on Pt/ZrO_2-5S under reaction conditions might also contribute to its enhanced propane combustion activity. Therefore, Pt/ZrO_2-5S reduced by H_2 at 200 °C (denoted as Pt/ZrO_2-5S-R) outperforms pristine Pt/ZrO_2-5S during the heating run, as shown in Figure S12. In the cooling run, the activity on Pt/ZrO_2-5S was significantly enhanced and became comparable to that of Pt/ZrO_2-5S-R, which should be due to the *in situ* generation of abundant Pt^0 species in Pt/ZrO_2-5S under the reaction conditions.

3.4. Reaction Mechanism. Results of kinetic experiments and *in* situ DRIFTS of propane combustion are presented in Figure 5 and Tables S2−S5. The apparent activation energy of the propane combustion reaction on Pt/ZrO_2 (84.2 ± 10.0 kJ·mol^{-1}) was much higher than that on Pt/ZrO_2-5S (54.6 ± 5.3 kJ·mol^{-1}), suggesting that sulfate species could facilitate the activation of reactants (Figure 5a). Although both Pt/ZrO_2 (1.03 ± 0.01) and Pt/ZrO_2-5S (1.06 ± 0.02) exhibited positive and comparable propane reaction orders (Figure 5b), their O_2 reaction orders differed markedly. Specifically, Pt/ZrO_2 (−0.57 ± 0.05) showed a negative order, while Pt/ZrO_2-5S (0.54 ± 0.04) displayed a positive order (Figure 5c). That is, the severe competitive adsorption between propane and O_2 on Pt/ZrO_2 catalysts was significantly alleviated by the sulfate modification.

https://doi.org/10.1021/acscatal.5c06403
ACS Catal. 2025, 15, 21054−21065

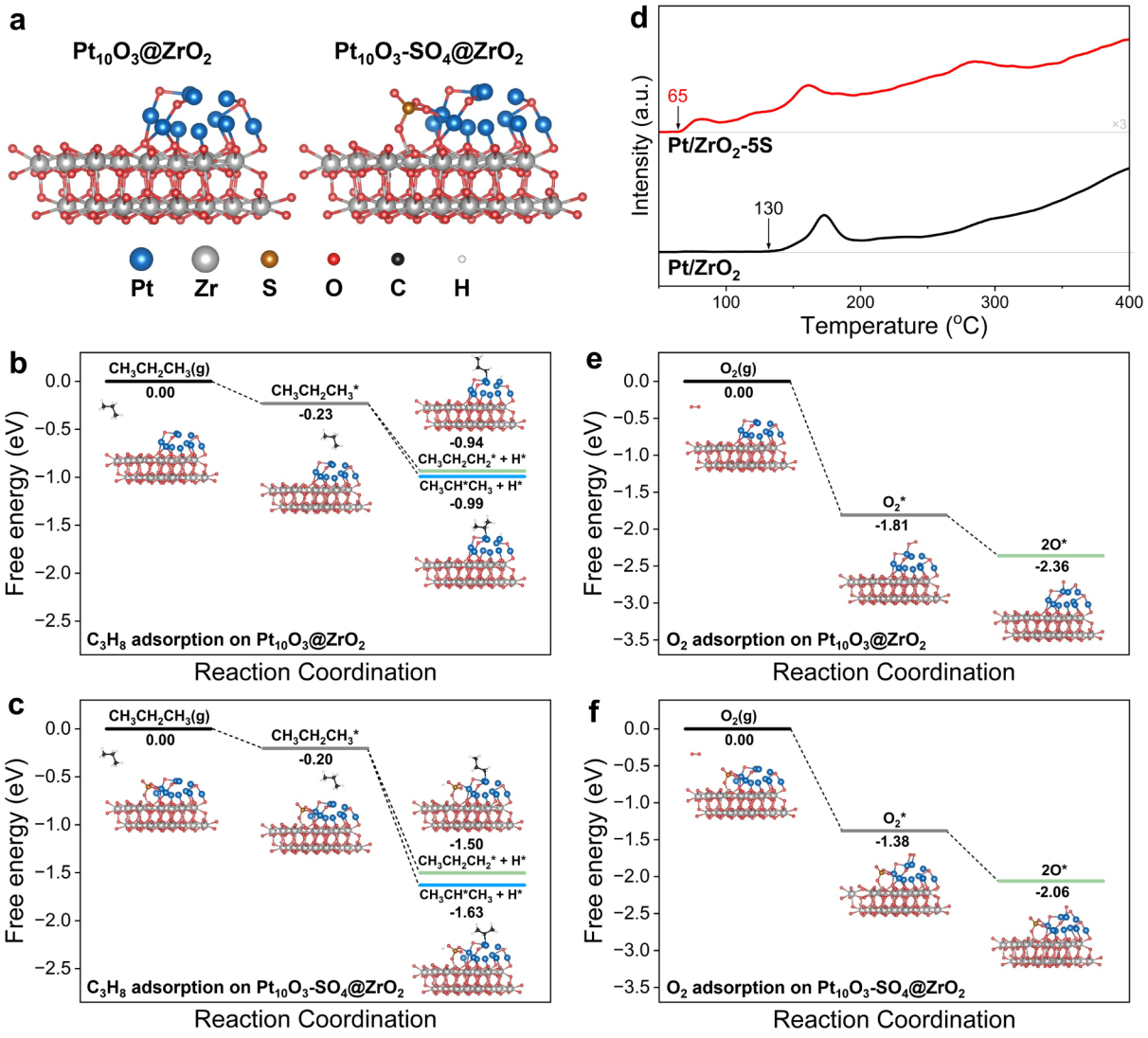

Figure 6. a) Structure models of the $Pt_{10}O_3$ cluster on t-ZrO_2 (011) without and with an adjacent sulfate group (left: $Pt_{10}O_3$@ZrO_2, right: $Pt_{10}O_3$–SO_4@ZrO_2). Gibbs free energy (ΔG) profiles for the adsorption of propane and activated propane on b) $Pt_{10}O_3$@ZrO_2 and c) $Pt_{10}O_3$–SO_4@ZrO_2. d) Temperature-programmed reactions on Pt/ZrO_2 and Pt/ZrO_2-5S in C_3H_8 flow. Gibbs free energy (ΔG) profiles for the O_2 adsorption and dissociation on e) $Pt_{10}O_3$@ZrO_2 and f) $Pt_{10}O_3$–SO_4@ZrO_2.

Specifically, weakened O_2 adsorption and strengthened propane dissociation/adsorption might be achieved on Pt/ZrO_2-5S.

In situ DRIFTS of propane combustion was performed on Pt/ZrO_2 and Pt/ZrO_2-5S from 100 to 380 °C to further investigate the reaction mechanism, as shown in Figure 5d-e. The characteristic peaks at 1542 and 1460 cm^{-1} were observed on Pt/ZrO_2, which were ascribed to the formate species (CH_3COO*).[66] CO (2100 and 2000 cm^{-1}) adsorbed on PtO_x or Pt^0 sites and C–H in C_3H_8 (2967 cm^{-1}) were also observed. For Pt/ZrO_2-5S, in addition to formate species, multiple intermediates, including methoxy species (–OCH_3, 1102 cm^{-1}), CH_3COO* (1460, 1560 cm^{-1}), CO (2080 cm^{-1}) adsorbed on Pt^0 sites, –OH (3233 cm^{-1}), and C–H in C_3H_8 (2967 cm^{-1})[41,66] emerged as well, indicating that propane was more prone to cracking on Pt/ZrO_2-5S compared to Pt/ZrO_2, and the possible weakened O_2 adsorption on sulfate-modified Pt sites might facilitate the adsorption of reaction intermediates. In addition, the easier cracking of C_3H_8 and the formation of reductive intermediates on Pt/ZrO_2-5S might also facilitate the generation of Pt^0 species under the reaction conditions. The observations described above demonstrated that the reaction behaviors of propane combustion on Pt/ZrO_2 were significantly altered by sulfate modification.

In order to deeply understand the critical roles of sulfates in reactant adsorption and activation on Pt/ZrO_2, DFT calculations were conducted (Figure 6, Figure S13–16). According to the results of TEM and XPS, the ZrO_2 support in Pt/ZrO_2-5S preferentially exposed t-ZrO_2 (011) facet, and the supported Pt clusters in spent catalyst (spent Pt/ZrO_2-5S) were in mixed valence states (ca. 35% $Pt^{\delta+}$). Two structural models of $Pt_{10}O_3$ clusters supported on t-ZrO_2 (011) facet without and with an adjacent sulfate group were proposed for mechanism investigation. These models were denoted as $Pt_{10}O_3$@ZrO_2 and $Pt_{10}O_3$–SO_4@ZrO_2, respectively (Figure 6a).

Since the competitive adsorption between propane and O_2 would determine the catalytic performance of Pt/ZrO_2 catalysts in the propane combustion reaction, the Gibbs free energy change (ΔG) of propane and O_2 adsorption over

https://doi.org/10.1021/acscatal.5c06403
ACS Catal. 2025, 15, 21054–21065

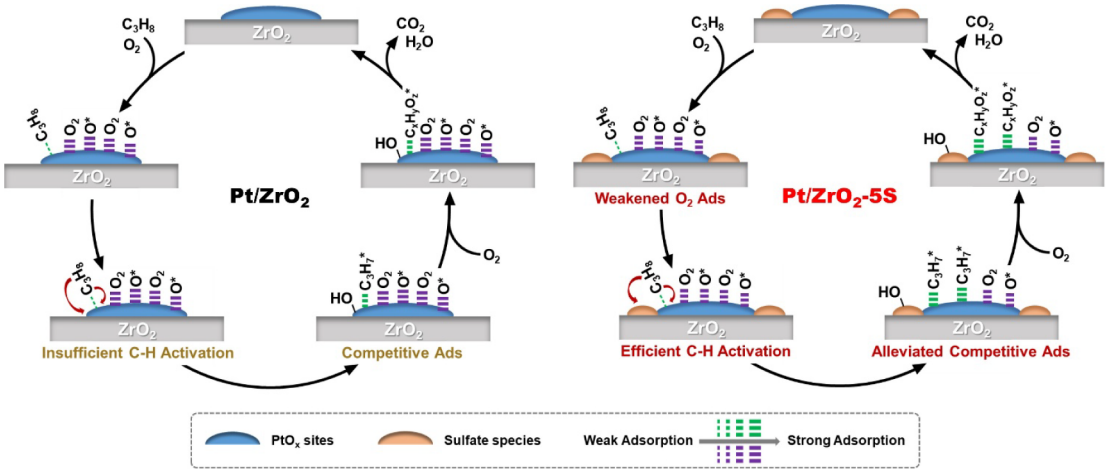

Figure 7. Proposed reaction mechanisms of the propane combustion reaction over Pt/ZrO_2 and Pt/ZrO_2-5S catalysts (Ads = Adsorption, -$C_xH_yO_z$* = intermediates from propane).

$Pt_{10}O_3$@ZrO_2 and $Pt_{10}O_3$−SO_4@ZrO_2 was first calculated by DFT. As shown in Figure 6b and 6c, the adsorption energy of propane on $Pt_{10}O_3$ cluster and sulfate-modified $Pt_{10}O_3$ cluster was −0.23 and −0.20 eV, respectively. Such weak adsorption indicated that further activation was required to facilitate the adsorption and deep oxidation of propane. Additionally, the DRIFTS study of C_3H_8 adsorption on Pt/ZrO_2 and Pt/ZrO_2-5S at room temperature (25 °C) and C_3H_8-TPD further confirmed that C_3H_8 without further activation could not be stably adsorbed on Pt/ZrO_2 and sulfated Pt/ZrO_2 catalysts (Figures S17 and S18). Based on this understanding, the ΔG value for the adsorption of propane after the cleavage of the C−H bond from $-CH_3$ ($CH_3CH_2CH_2$*) or $-CH_2-$ (CH_3CH*CH_3) was explored. It was noteworthy that the adsorption energy of $CH_3CH_2CH_2$* + H* and CH_3CH*CH_3 + H* on $Pt_{10}O_3$ (−0.94 and −0.99 eV) was higher than that on sulfate-modified $Pt_{10}O_3$ (−1.50 and −1.63 eV), which meant that sulfate modification could significantly promote the adsorption of activated propane on PtO_x clusters. Besides, the adsorption of CH_3CH*CH_3 was slightly stronger than that of $CH_3CH_2CH_2$*, and the optimization process suggested that the dissociated H* would migrate to the adjacent sulfate group.

Due to the high degrees of freedom of the propane molecule, the accurate theoretical determination of the propane activation energy on $Pt_{10}O_3$ clusters presents a significant challenge. Instead, the propane dehydrogenation performance of Pt/ZrO_2 and Pt/ZrO_2-5S was evaluated using temperature-programmed reactions in a C_3H_8 flow to directly compare their C−H activation capabilities. As shown in Figure 6d, propene was generated on Pt/ZrO_2-5S at much lower temperatures (65 °C) compared to Pt/ZrO_2 (130 °C), indicating that sulfate species would effectively facilitate the activation of C−H in propane on Pt sites.

ΔG for O_2 adsorption on $Pt_{10}O_3$@ZrO_2 and $Pt_{10}O_3$−SO_4@ZrO_2 was also calculated (Figures 6e and 6f). As expected, the adsorption energy of O_2 on the $Pt_{10}O_3$ cluster (−1.81 eV) was much lower than that on the sulfate-modified $Pt_{10}O_3$ cluster (−1.38 eV), confirming that the strength of the adsorption of O_2 on Pt sites was significantly suppressed by sulfate modification. Moreover, after the dissociation of O_2, the ΔG value for the two O* adsorbed on the $Pt_{10}O_3$ cluster is −2.36 eV, still lower than that on the sulfate-modified $Pt_{10}O_3$ cluster (−2.06 eV), further indicating that the sulfate species could weaken the adsorption of oxygen species. It could be concluded from DFT calculations and temperature-programmed reactions that the sulfate modification significantly enhanced the adsorption/activation of propane while suppressing the adsorption of O_2 on Pt sites, a trend consistent with the kinetics study.

Drawing on the experimental and theoretical results, the reaction mechanism for propane combustion over Pt/ZrO_2 and Pt/ZrO_2-5S was proposed from the perspective of reactant competitive adsorption and activation, as shown in Figure 7. For the Pt/ZrO_2 catalyst, its relatively poor catalytic performance was primarily due to insufficient C−H activation of propane, coupled with the weak competitive adsorption of activated propane against O_2 on the Pt active sites. In clear contrast, the synergy between sulfate species and Pt sites on Pt/ZrO_2-5S not only facilitated the activation of C−H but also mediated the competitive adsorption between activated propane and O_2 through weakening the adsorption of O_2 and enhancing the adsorption of activated propane/intermediates. Consequently, the propane combustion reaction could be effectively catalyzed by the Pt/ZrO_2-5S.

4. CONCLUSION

In this study, a robust sulfate-modified Pt/ZrO_2 catalyst for propane combustion was constructed by depositing Pt onto a sulfated ZrO_2 support prepared by an environmentally friendly one-step pyrolysis method. To elucidate the fundamental reasons for the significantly enhanced propane combustion activity on Pt/ZrO_2 induced by sulfate modification from the perspective of adsorption behavior of reactants, systematic characterizations, kinetic studies, and DFT calculations were conducted. It was revealed that sulfate modification effectively alleviated the severe competitive adsorption between propane (weakly adsorbed) and O_2 (strongly adsorbed) on Pt active sites, a key limitation leading to inferior activity in the unmodified Pt/ZrO_2 catalyst. Specifically, sulfate incorporation enhanced the activation/adsorption of propane and its resulting intermediates while simultaneously weakening oxygen binding, thereby markedly improving the catalytic activity for propane combustion, with T_{90} decreasing from 320 to 200 °C. These findings provided deep insights into the adsorption-mediated reaction mechanism and offered a strategic direction

https://doi.org/10.1021/acscatal.5c06403
ACS Catal. 2025, 15, 21054−21065

for the rational design of efficient catalysts for alkane combustion.

■ ASSOCIATED CONTENT

Supporting Information

The Supporting Information is available free of charge at https://pubs.acs.org/doi/10.1021/acscatal.5c06403.

Synthesis of reference Pt/ZrO_2 catalysts, schematic diagram for synthesis of sulfate-modified Pt/ZrO_2, TG plots, XRD patterns, Raman spectra, activity tests on reference Pt/ZrO_2 catalysts, HRTEM images, XPS, high-resolution images of propane/O_2 adsorption configurations on catalyst, data for activation energy and reaction order calculation, *in situ* DRIFTS of propane adsorption, C_3H_8-TPD (PDF)

■ AUTHOR INFORMATION

Corresponding Authors

Wen-Zhi Jia − *Huzhou Key Laboratory of Environmental Functional Materials and Pollution Control, Department of Materials Engineering, Huzhou University, Huzhou 313000, China*; Email: jiawenzhi@126.com

Wei Tan − *State Key Laboratory of Water Pollution Control and Green Resource Recycling, School of Environment, Jiangsu Key Laboratory of Vehicle Emissions Control, Centre for Shared Scientific Research Facilities, Key Laboratory of Mesoscopic Chemistry of MOE, School of Chemistry and Chemical Engineering, Nanjing University, Nanjing 210023, China*; orcid.org/0000-0002-1481-9346; Email: tanwei@nju.edu.cn

Jian Chen − *Key Laboratory of the Ministry of Education for Advanced Catalysis Materials, Zhejiang Key Laboratory of Advanced Catalysis and Adsorption Materials, Zhejiang Normal University, Jinhua 321004, China*; orcid.org/0000-0001-5982-044X; Email: jianchen@zjnu.cn

Authors

Han Zhao − *Key Laboratory of the Ministry of Education for Advanced Catalysis Materials, Zhejiang Key Laboratory of Advanced Catalysis and Adsorption Materials, Zhejiang Normal University, Jinhua 321004, China*

Lu Liu − *Key Laboratory of the Ministry of Education for Advanced Catalysis Materials, Zhejiang Key Laboratory of Advanced Catalysis and Adsorption Materials, Zhejiang Normal University, Jinhua 321004, China*

Yao-Dong Hao − *Key Laboratory of the Ministry of Education for Advanced Catalysis Materials, Zhejiang Key Laboratory of Advanced Catalysis and Adsorption Materials, Zhejiang Normal University, Jinhua 321004, China*

Xiao-Yang Zhu − *Key Laboratory of Integrated Regulation and Resource Development on Shallow Lakes, Ministry of Education, College of Environment, Hohai University, Nanjing 210098, China*

Qian Zhou − *Key Laboratory of the Ministry of Education for Advanced Catalysis Materials, Zhejiang Key Laboratory of Advanced Catalysis and Adsorption Materials, Zhejiang Normal University, Jinhua 321004, China*

Yi-Wei Xian − *Key Laboratory of the Ministry of Education for Advanced Catalysis Materials, Zhejiang Key Laboratory of Advanced Catalysis and Adsorption Materials, Zhejiang Normal University, Jinhua 321004, China*

Lin Dong − *State Key Laboratory of Water Pollution Control and Green Resource Recycling, School of Environment, Jiangsu Key Laboratory of Vehicle Emissions Control, Centre for Shared Scientific Research Facilities, Key Laboratory of Mesoscopic Chemistry of MOE, School of Chemistry and Chemical Engineering, Nanjing University, Nanjing 210023, China*; orcid.org/0000-0002-8393-6669

Meng-Fei Luo − *Key Laboratory of the Ministry of Education for Advanced Catalysis Materials, Zhejiang Key Laboratory of Advanced Catalysis and Adsorption Materials, Zhejiang Normal University, Jinhua 321004, China*; orcid.org/0000-0002-9331-701X

Complete contact information is available at: https://pubs.acs.org/10.1021/acscatal.5c06403

Author Contributions

#H.Z. and L.L. contributed equally to this work.

Notes

The authors declare no competing financial interest.

■ ACKNOWLEDGMENTS

This work was financially supported by the National Natural Science Foundation of China (No. 22172145, 22306090), the Leading Innovative and Entrepreneur Team Introduction Program of Zhejiang (No. 2022R01007), the Natural Science Foundation of Jiangsu Province (BK20230773, BK20231513), Research Fund of Key Laboratory of the Ministry of Education for Advanced Catalysis Materials and Zhejiang Key Laboratory of Advanced Catalysis and Adsorption Materials, Zhejiang Normal University.

■ REFERENCES

(1) Zhang, L.; Chu, P.; Wang, Y.; Tao, J.; Han, Y.; Shi, Y.; Guo, M.; Wang, S.; Liu, Y.; Dai, H.; et al. Promotion effect of strong CeO_2/Co_3O_4 interfacial interaction for light alkane catalytic removal. *Appl. Catal. B* **2025**, *369*, 125150.

(2) Yang, S.; Zhang, M.; Li, H.; Gao, J.; Li, W.; Chen, L.; Zhang, S.; Li, W.; Li, S. Phosphate-induced electronic tuning of MnO_2: Unlocking enhanced activation and complete oxidation of propane. *Appl. Catal. B* **2025**, *372*, 125291.

(3) Zhu, Z.; Lu, G.; Guo, Y.; Guo, Y.; Zhang, Z.; Wang, Y.; Gong, X.-Q. High performance and stability of the Pt-W/ZSM-5 catalyst for the total oxidation of propane: The role of tungsten. *ChemCatchem* **2013**, *5* (8), 2495−2503.

(4) Huang, Z.; Cao, S.; Yu, J.; Tang, X.; Guo, Y.; Guo, Y.; Wang, L.; Dai, S.; Zhan, W. Total oxidation of light alkane over phosphate-modified Pt/CeO_2 catalysts. *Environ. Sci. Technol.* **2022**, *56* (13), 9661−9671.

(5) Wang, A.; Ding, J.; Li, M.; Song, P.; Zhao, Z.; Guo, Y.; Guo, Y.; Wang, L.; Dai, Q.; Zhan, W. robust Ru/Ce@Co catalyst with an optimized support structure for propane oxidation. *Environ. Sci. Technol.* **2024**, *58* (28), 12742−12753.

(6) Liu, Y.; Hu, H.; Zheng, J.; Xie, F.; Gu, H.; Rostamnia, S.; Pan, F.; Liu, X.; Zhang, L. Interfacial engineering enables surface lattice oxygen activation of $SmMn_2O_5$ for catalytic propane combustion. *Appl. Catal. B* **2023**, *330*, 122649.

(7) Zhu, W.; Chen, X.; Li, C.; Liu, Z.; Liang, C. Manipulating morphology and surface engineering of spinel cobalt oxides to attain high catalytic performance for propane oxidation. *J. Catal.* **2021**, *396*, 179−191.

(8) Zhang, T.; Lang, X.; Dong, A.; Wan, X.; Gao, S.; Wang, L.; Wang, L.; Wang, W. Difference of oxidation mechanism between light C3−C4 alkane and alkene over mullite YMn_2O_5 oxides' catalyst. *ACS Catal.* **2020**, *10* (13), 7269−7282.

(9) Dong, J.; Li, D.; Zhang, Y.; Chang, P.; Jin, Q. Insights into the CeO_2 facet-depended performance of propane oxidation over Pt-CeO_2 catalysts. *J. Catal.* **2022**, *407*, 174−185.
(10) Wang, R.; Li, G.; Zong, X.; Wang, J.; Xu, Y.; Jin, C.; Wang, M.; Ma, P.; Zhang, R.; Zheng, K.; et al. Electron withdrawal from methane by Pt atoms on stannic oxide for highly active low-temperature combustion. *Environ. Sci. Technol.* **2025**, *59* (24), 12121−12131.
(11) Song, S.; Wen, M.; Zhao, W.; Kong, J.; Li, G.; An, T. Modulation mechanism of Mn-O strength in α-MnO_2 catalyst for high-efficiency catalytic combustion of propane. *Appl. Catal. B* **2024**, *354*, 124120.
(12) Ma, X.; Tang, Y.; Liu, Y.; Zhang, Y.; Jia, L.; Liu, X.; Du, C.; Shan, B. A-site cation exfoliation of amorphous $SmMn_xO_y$ oxides for low temperature propane oxidation. *J. Catal.* **2022**, *409*, 59−69.
(13) Gu, H.; Wang, F.; Chen, S.; Lan, J.; Wang, J.; Pei, C.; Liu, X.; Gong, J. Suppressing Jahn-Teller distortion of MnO_2 via B-Ni dual single-atoms integration for methane catalytic combustion. *Nat. Commun.* **2025**, *16* (1), 1008.
(14) Mu, G.; Xie, H.; Jian, Y.; Jiang, Z.; Li, L.; Tian, M.; Zhang, L.; Wang, J.; Chai, S.; He, C. Facile construction and enhanced catalytic activity of Co-Mn oxide with rich amorphous/crystalline interfaces for propane oxidation. *Sep. Purif. Technol.* **2024**, *348*, 127699.
(15) Mao, X.; Liu, S.; Liu, W.; Wu, X.; Liu, S. A simple model catalyst study to distinguish the roles of different oxygen species in propane and soot combustion. *Appl. Catal. B* **2022**, *310*, 121331.
(16) Wang, J.; Jiang, Z.; Xu, H.; Li, X.; Jian, Y.; Xia, L.; Su, P.; Liu, Q.; Chai, S.; Ma, M.; et al. Elucidating confinement and micro-environment of Ru clusters stably confined in MFI Zeolite for efficient propane oxidation. *Angew. Chem., Int. Ed.* **2025**, *64* (5), No. e202417618.
(17) Wu, X.; Zhang, L.; Weng, D.; Liu, S.; Si, Z.; Fan, J. Total oxidation of propane on Pt/WOx/Al2O3 catalysts by formation of metastable $Pt^{\delta+}$ species interacted with WOx clusters. *J. Hazard Mater.* **2012**, *225-226*, 146−154.
(18) Liu, Y.-R.; Li, X.; Liao, W.-M.; Jia, A.-P.; Wang, Y.-J.; Luo, M.-F.; Lu, J.-Q. Highly active Pt/BN catalysts for propane combustion: The roles of support and reactant-induced evolution of active sites. *ACS Catal.* **2019**, *9* (2), 1472−1481.
(19) Enterkin, J. A.; Setthapun, W.; Elam, J. W.; Christensen, S. T.; Rabuffetti, F. A.; Marks, L. D.; Stair, P. C.; Poeppelmeier, K. R.; Marshall, C. L. Propane oxidation over Pt/$SrTiO_3$ nanocuboids. *ACS Catal.* **2011**, *1* (6), 629−635.
(20) Chai, H.; Xu, J.; Zhang, Z.; Lai, J.-A.; Wang, J.; Peng, Z.; Liu, K.; Rao, C.; Xie, H.; Liu, Q.; et al. Tuning surface defects of WO_{3-x} for enhanced photothermal catalytic propane combustion. *Appl. Surf. Sci.* **2024**, *657*, 159709.
(21) Jian, Y.; Xu, H.; Wang, Y.; Wang, J.; Xia, L.; Liu, Y.; Yu, Y.; He, C. Chromium promoted the efficient and stable catalytic degradation of propane over Pt/HZSM-5 catalyst: Optimization and reaction mechanism. *Appl. Surf. Sci.* **2025**, *699*, 163149.
(22) Yu, Z.; Fang, Y.; Pan, C.; Ma, S.; Zeng, Y.; Yang, J.; Wan, S.; Zhong, Z. Construction of electron-enriched $Pt^{\delta+}$ with reactive oxygen species for enhanced propane catalytic combustion. *ACS Appl. Mater. Interfaces* **2025**, *17* (14), 21246−21256.
(23) Lambert, C. K. Current state of the art and future needs for automotive exhaust catalysis. *Nat. Catal.* **2019**, *2* (7), 554−557.
(24) Yang, A.-C.; Streibel, V.; Choksi, T. S.; Aljama, H.; Werghi, B.; Bare, S. R.; Sánchez-Carrera, R. S.; Schäfer, A.; Li, Y.; Abild-Pedersen, F.; et al. Insights and comparison of structure−property relationships in propane and propene catalytic combustion on Pd- and Pt-based catalysts. *J. Catal.* **2021**, *401*, 89−101.
(25) Zhao, P.-P.; Chen, J.; Yu, H.-B.; Cen, B.-H.; Wang, W.-Y.; Luo, M.-F.; Lu, J.-Q. Insights into propane combustion over MoO_3 promoted Pt/ZrO_2 catalysts: The generation of Pt-MoO_3 interface and its promotional role on catalytic activity. *J. Catal.* **2020**, *391*, 80−90.
(26) Ge, S.; Fan, W.; Tang, X.; Cui, Y.; Wang, D.; Gong, X.-Q.; Dai, S.; Lou, Y.; Tang, J.; Guo, Y.; et al. Revealing the size effect of ceria nanocube-supported platinum nanoparticles in complete propane oxidation. *ACS Catal.* **2024**, *14* (4), 2532−2544.
(27) Avila, M. S.; Vignatti, C. I.; Apesteguía, C. R.; Garetto, T. F. Effect of support on the deep oxidation of propane and propylene on Pt-based catalysts. *Chem. Eng. J.* **2014**, *241*, 52−59.
(28) You, Y.; Xu, A.; Tang, X.; Guo, Y.; Zhan, W.; Wang, L.; Dai, S.; Guo, Y. Refining metal−support interactions via surface modification of irreducible oxide support for enhanced complete propane oxidation. *ACS Catal.* **2024**, *14* (15), 11457−11467.
(29) Shao, C.; Yang, J.; You, Y.; Tang, X.; Tang, J.; Wang, L.; Cui, Y.; Zhan, W.; Guo, Y.; Guo, Y. Regulating the selective dispersion of tungsten oxide to promote propane combustion on Pt-nanoparticle catalysts supported on WO_x/ZrO_2 by tuning the zirconia crystal phase. *ACS Appl. Nano Mater.* **2022**, *5* (9), 13482−13497.
(30) Xia, L.; Jian, Y.; Liu, Q.; Liu, Y.; Wang, J.; Chai, S.; Jing, M.; Albilali, R.; He, C. Boosted light alkane deep oxidation via metal bond length modulation-induced C−C bond preferential activation. *Environ. Sci. Technol.* **2024**, *58* (7), 3472−3482.
(31) Yang, A.-C.; Zhu, H.; Li, Y.; Cargnello, M. Support acidity improves Pt activity in propane combustion in the presence of steam by reducing water coverage on the active sites. *ACS Catal.* **2021**, *11* (11), 6672−6683.
(32) Yazawa, Y.; Takagi, N.; Yoshida, H.; Komai, S.-I.; Satsuma, A.; Tanaka, T.; Yoshida, S.; Hattori, T. The support effect on propane combustion over platinum catalyst: control of the oxidation-resistance of platinum by the acid strength of support materials. *Appl. Catal., A* **2002**, *233* (1), 103−112.
(33) Yazawa, Y.; Yoshida, H.; Hattori, T. The support effect on platinum catalyst under oxidizing atmosphere: improvement in the oxidation-resistance of platinum by the electrophilic property of support materials. *Appl. Catal., A* **2002**, *237* (1), 139−148.
(34) Huang, Z.; Ding, J.; Yang, X.; Liu, H.; Song, P.; Guo, Y.; Guo, Y.; Wang, L.; Zhan, W. Highly efficient oxidation of propane at low temperature over a Pt-based catalyst by optimization support. *Environ. Sci. Technol.* **2022**, *56* (23), 17278−17287.
(35) Kovalyov, E. V.; Sadovskaya, E. M.; Bal'zhinimaev, B. S. Kinetic features of the deep oxidation of propane over a Pt/fiberglass catalyst. *Chem. Eng. J.* **2018**, *349*, 547−553.
(36) Chen, W.; Liu, C.; Lian, C.; Yu, Y.; Zhang, X.; Qian, G.; Yang, J.; Chen, D.; Zhou, X.; Yuan, W.; et al. Engineering electronic platinum−carbon support interaction to tame carbon monoxide activation. *Fundam. Res.* **2024**, *4* (5), 1118−1127.
(37) Huang, M.; Li, Y.; Li, M.; Zhao, J.; Zhu, Y.; Wang, C.; Sharma, V. K. Active site-directed tandem catalysis on single platinum nanoparticles for efficient and stable oxidation of formaldehyde at room temperature. *Environ. Sci. Technol.* **2019**, *53* (7), 3610−3619.
(38) Dong, J.; Li, T.; Li, S.; Chang, P.; Jin, Q.; Yang, J.; Lai, Z. Local environment and electronic structure of Pt-TiO_2 catalysts define the reactivity of CO oxidation and C_3H_8 combustion: the crystal phase of TiO_2 determining. *ACS Catal.* **2025**, *15*, 15794−15807.
(39) Chen, W.; Zheng, J.; Fang, Y.; Wang, Y.; Hu, J.; Zhu, Y.; Zhu, X.; Li, W.; Zhang, Q.; Pan, C.; et al. Role of the in-situ-formed surface (Pt−S−O)-Ti active structure in SO_2-promoted C_3H_8 combustion over a Pt/TiO_2 catalyst. *Environ. Sci. Technol.* **2024**, *58* (6), 3041−3053.
(40) Shao, C.; Cui, Y.; Zhang, L.; Tang, J.; Ge, C.; Chen, B.; Wang, L.; Guo, Y.; Zhan, W.; Guo, Y. Boosting propane purification on Pt/$ZrOSO_4$ nanoflowers: Insight into the roles of different sulfate species in synergy with Pt. *Sep. Purif. Technol.* **2023**, *304*, 122367.
(41) Li, D.-D.; Leng, X.-Y.; Wang, X.-F.; Yu, H.-B.; Zhang, W.-Q.; Chen, J.; Lu, J.-Q.; Luo, M.-F. Unraveling the promoting roles of sulfate groups on propane combustion over Pt-SO_4^{2-}/ZrO_2 catalysts. *J. Catal.* **2022**, *407*, 322−332.
(42) Hao, H.; Jin, B.; Liu, W.; Wu, X.; Yin, F.; Liu, S. Robust Pt@TiO_x/TiO_2 catalysts for hydrocarbon combustion: Effects of Pt-TiO_x interaction and sulfates. *ACS Catal.* **2020**, *10* (22), 13543−13548.
(43) Zhang, L.; Weng, D.; Wang, B.; Wu, X. Effects of sulfation on the activity of $Ce_{0.67}Zr_{0.33}O_2$ supported Pt catalyst for propane oxidation. *Catal. Commun.* **2010**, *11* (15), 1229−1232.

https://doi.org/10.1021/acscatal.5c06403
ACS Catal. 2025, 15, 21054−21065

(44) Gu, L.; Chen, X.; Zhou, Y.; Zhu, Q.; Huang, H.; Lu, H. Propene and CO oxidation on Pt/Ce-Zr-SO_4^{2-} diesel oxidation catalysts: Effect of sulfate on activity and stability. *Chin. J. Catal.* **2017**, *38* (3), 607−615.
(45) Wang, B.; Wu, X.; Ran, R.; Si, Z.; Weng, D. Participation of sulfates in propane oxidation on Pt/SO_4^{2-}/CeO_2−ZrO_2 catalyst. *J. Mol. Catal. A: Chem.* **2012**, *361*−*362*, 98−103.
(46) Wang, X.-F.; Xu, L.-Y.; Wen, C.-H.; Li, D.-D.; Li, B.; Lu, J.-Q.; Yang, Q.-H.; Luo, M.-F.; Chen, J. WO_3 boosted water tolerance of Pt nanoparticle on SO_4^{2-}-ZrO_2 for propane oxidation. *Appl. Catal., B* **2023**, *338*, 123000.
(47) Wu, Y.; Liao, S. Review of SO_4^{2-}/M_xO_y solid superacid catalysts. *Front. Chem. Eng. China* **2009**, *3* (3), 330−343.
(48) Dun, Y.; Liu, Y.; Xu, J.; Xie, L.; Du, C.; Wang, C.; Zhao, Y.; Liu, F.; Chen, R.; Shan, B. Pt^0-$MnSO_4$ active centers on modified $SmMn_2O_5$ mullite oxides for efficient propane oxidation. *Appl. Catal. B* **2025**, *371*, 125223.
(49) Wu, S.; Feng, C.; Dong, F.; Ma, S.; Han, W.; Han, W.; Zhang, H.; Tang, Z. Tailored $CoNiO_x$@$CuVO_x$ core-shell catalyst exhibiting strong charge transfer and SO_2 tolerance for efficient elimination of propane. *Appl. Catal. B* **2025**, *372*, 125293.
(50) Fu, Q.; Wang, S.; Wang, T.; Xing, D.; Yue, X.; Wang, M.; Wang, S. Insights into the promotion mechanism of ceria-zirconia solid solution to ethane combustion over Pt-based catalysts. *J. Catal.* **2022**, *405*, 129−139.
(51) Kresse, G.; Furthmüller, J. Efficiency of ab-initio total energy calculations for metals and semiconductors using a plane-wave basis set. *Comput. Mater. Sci.* **1996**, *6* (1), 15−50.
(52) Kresse, G.; Furthmüller, J. Efficient iterative schemes for ab initio total-energy calculations using a plane-wave basis set. *Phys. Rev. B* **1996**, *54* (16), 11169−11186.
(53) Perdew, J. P.; Burke, K.; Ernzerhof, M. Generalized gradient approximation made simple. *Phys. Rev. Lett.* **1996**, *77* (18), 3865−3868.
(54) Kresse, G.; Joubert, D. From ultrasoft pseudopotentials to the projector augmented-wave method. *Phys. Rev. B* **1999**, *59* (3), 1758−1775.
(55) Blöchl, P. E. Projector augmented-wave method. *Phys. Rev. B* **1994**, *50* (24), 17953−17979.
(56) Grimme, S.; Antony, J.; Ehrlich, S.; Krieg, H. A consistent and accurate ab initio parametrization of density functional dispersion correction (DFT-D) for the 94 elements H-Pu. *J. Chem. Phys.* **2010**, *132* (15), 154104.
(57) Pinheiro, M. G. S.; Chagas, L. H.; Souza, E. F.; Gonzalez, G. G.; Zonetti, P. C.; Alves, O. C.; Rossi, L. M.; Pandoli, O. G.; de Avillez, R. R.; Borges, L. E. P.; et al. Role of oxygen vacancies employing $Ga_xZr_{1-x}O_{2-y}$/ZrO_2 in isobutene generation from ethanol. *J. Catal.* **2025**, *448*, 116205.
(58) Rabee, A. I. M.; Zhao, D.; Cisneros, S.; Kreyenschulte, C. R.; Kondratenko, V.; Bartling, S.; Kubis, C.; Kondratenko, E. V.; Brückner, A.; Rabeah, J. Role of interfacial oxygen vacancies in low-loaded Au-based catalysts for the low-temperature reverse water gas shift reaction. *Appl. Catal. B* **2023**, *321*, 122083.
(59) Jin, M.; Xu, B.; Ma, J.; Yi, C.; Liu, Y. Manipulating the surface oxygen vacancies of the nanosized ZrO_2 carrier for Co-catalyzed Fischer−Tropsch synthesis. *ACS Sustainable Chem. Eng.* **2025**, *13* (9), 3741−3751.
(60) Wang, W.; Song, S.; Wang, P.; He, M.; Fang, Z.; Yuan, X.; Li, H.; Li, C.; Wang, X.; Wei, Y.; et al. Chemical Bonding of g-C_3N_4/UiO-66(Zr/Ce) from Zr and Ce Single Atoms for Efficient Photocatalytic Reduction of CO_2 under Visible Light. *ACS Catal.* **2023**, *13* (7), 4597−4610.
(61) Yang, S.; Guo, X.; Li, X.; Wu, T.; Zou, L.; He, Z.; Xu, Q.; Zheng, J.; Chen, L.; Wang, Q.; Xu, Z. J.; et al. Enhancing photocatalytic CO_2 conversion through oxygen-vacancy-mediated topological phase transition. *Angew. Chem., Int. Ed.* **2024**, *63* (11), No. e202317957.
(62) Zhou, Y.; Liu, L.; Li, G.; Hu, C. Insights into the influence of ZrO_2 crystal structures on methyl laurate hydrogenation over Co/ZrO_2 catalysts. *ACS Catal.* **2021**, *11* (12), 7099−7113.
(63) Li, X.; Liu, Y.-R.; Liao, W.-M.; Jia, A.-P.; Wang, Y.-J.; Lu, J.-Q.; Luo, M.-F. Synergistic roles of Pt^0 and Pt^{2+} species in propane combustion over high-performance Pt/AlF_3 catalysts. *Appl. Surf. Sci.* **2019**, *475*, 524−531.
(64) Xian, Y.-W.; Li, B.; Wen, C.-H.; Xu, L.-Y.; Lu, W.-X.; Zhou, Q.; Jia, W.-Z.; Luo, M.-F.; Chen, J. Boosting propane combustion on dual active sites of Pt/WO_3 through regulating Pt sites and activating propane on WO_3 surface. *Fuel* **2025**, *385*, 134172.
(65) Burch, R.; H, M. J. C-H bond activation in hydrocarbon oxidation on solid catalysts. *J. Mol. Catal. A: Chem.* **1995**, *100* (1−3), 13−33.
(66) O'Brien, C. P.; Lee, I. C. A detailed spectroscopic analysis of the growth of oxy-carbon species on the surface of Pt/Al_2O_3 during propane oxidation. *J. Catal.* **2017**, *347*, 1−8.

https://doi.org/10.1021/acscatal.5c06403
ACS Catal. 2025, 15, 21054−21065